JOURNAL OF Applied Polymer SCIENCE

Investigations on Rheological Properties and Gelation of Tasar Regenerated Silk Fibroin Solution

Yogesha Lakkegowda,[1,2] Raghu Ammannappa,[1,3] Sharath Ananthamurthy[1]
[1]Department of Physics, Jnanabharathi, Bangalore University, Bengaluru 560056, Karnataka, India
[2]Department of Physics, Government Science College, Hassan 573201, Karnataka, India
[3]Post Graduate Department of Physics, Government College (Autonomous), Mandya 571401, Karnataka, India
Correspondence to: S. Ananthamurthy (E-mail: asharath@gmail.com)

ABSTRACT: Tasar silk is a variety of non-mulberry silk indigenous to the Indian subcontinent. We present the measured frequency-dependent viscoelastic moduli of Tasar regenerated silk fibroin (RSF) solution using optical tweezers at two concentrations (0.16% and 0.25% w/v) and extend these measurements to the low frequency regime using a video microscopy technique. We extend the investigation on the rheological behavior of Tasar RSF for four more RSF concentrations, viz., 0.50%, 1.00%, 2.50% and 5.00% using video microscopy. In all the RSF samples, both storage and loss moduli are found to increase with frequency. At lower frequencies the loss modulus is more than the storage modulus and exhibit similar behavior until a crossover frequency beyond which the storage modulus exceeds the loss modulus at all frequencies. The relaxation time which is inversely related to the crossover frequency is found to rise sharply at 5% w/v, indicating the onset of gelation in the sample. These results are examined in relation to the viscoelastic parameters of mulberry silk, wherein the larger crossover frequencies at the same higher concentrations indicate relaxation times that are an order of magnitude smaller than those measured for Tasar RSF. © 2013 Wiley Periodicals, Inc. J. Appl. Polym. Sci. **2014**, *131*, 40104.

KEYWORDS: rheology; gels; microscopy; properties and characterization

Received 14 May 2013; accepted 11 October 2013
DOI: 10.1002/app.40104

INTRODUCTION

Silk, a fibrous protein polymer secreted as a continuous filament by silk worms and spiders, has attracted the interest of scientists and engineers for a long time.[1] Silk worms and spiders manufacture silk and use it to engineer structures of high strength, such as cocoons, webs and nets and this has motivated research in the search for artificial silk to manufacture in bulk quantity. Although the initial interest was motivated in manufacturing textiles of durability and aesthetic value, more recently the interest has extended to the use of silk as a valuable biotechnological material because of its compatibility with blood and its high permeability to both water and oxygen.[1] For use in a specific biomedical application, silk should be regenerated in a desirable form. By dissolving the silk fiber in a suitable solvent, a regenerated silk fibroin (RSF) polymer solution can be prepared.

Among the silk fibers secreted by silk worms, one may consider two classes of silks based on what the worm feeds on: mulberry, (the silk worm Bombyx mori feeds on this plant) and the other non-mulberry varieties. In the literature, a number of studies have been reported on the structure and mechanical properties of mulberry as well as non-mulberry silks, including the tensile stress–strain and recovery behavior of silk fibers under stress.[2] These studies reveal properties such as its high breaking extension and strength. Some of the findings from these investigations with regards to the properties such as toughness and stiffness are summarized in Table I. The microstructure of the Indian silk varieties has been elucidated through studies of their amino acid contents.[3] Stress relaxation in non-mulberry silk fibers is found to be significantly greater compared with that in mulberry silk.[4] Studies on the solubility and rheological behavior of mulberry RSF using a rheometer, at higher concentrations, have been reported[1] and their microrheological characterization has been carried out using video microscopy.[5]

Tasar silk fiber, white in color, comes from the worm *Antheraea-mylitta*, a natural fauna of tropical India. As indicated in Table I, it has lower stiffness but greater toughness than mulberry silk. Non-mulberry silk fibers also show higher moisture retention than mulberry silk fibers due to the higher ratio of hydrophilic to hydrophobic amino acid residues in the chemical structure of the former.[3] In this context it is worthwhile to examine whether

Additional Supporting Information may be found in the online version of this article.

Table I. Comparison of Some Properties of Tasar and Mulberry Silk varieties

	Property/silk variety	Tasar	Mulberry
Reference [2]	Stiffness/Modulus (gf/den)	66.68	87.50
	Toughness (gf/den)	0.98	0.3
Reference [3]	Density (g/cc)	1.32	1.35
	Moisture regain percentage	10.5	8.45

1gf/den = $(10^{-3} \times 1.13)$ N/tex = $(10^{-3} \times 1.13)$ Gpa/(g/cm^3).

the measured fiber stiffness and moisture retention ability have a bearing on the viscoelastic properties of their corresponding RSF solutions, facts that may be of significance in designing RSF based biomedical gels with specific rheological properties.

Silk hydrogels are networks of semiflexible biopolymers. Semiflexible polymers are those for which persistence length and the contour lengths have the same order of magnitude. These polymers tend to bend and entangle. Silk hydrogels are of technological interest because they demonstrate high elastic moduli at low polymer volume fractions.[6] A few studies on the gelation of silk solution process have been reported.[7–9] These studies using Fourier transform infrared (FTIR) spectroscopy and Circular Dichroism show that silk proteins have random coil conformation in solution form, and in the gel form, they change to β sheet conformation.[7,8] Further, it is shown that gelation mechanism from silk fibroin solution depends on temperature, pH and on concentration of silk proteins.[8] Studies on rheological behaviors of cross linked and non cross linked spider silk gels have been carried out.[9]

The details of microrheological techniques may be found elsewhere.[10–17] We briefly summarize the key features of this technique here. In microrheology, the position information of thermally fluctuating microscopic tracer beads embedded in a complex fluid are recorded.[13] Video microscopy is a passive technique in which the diffusion of a free bead in the sample medium is traced, whereas an optical tweezer uses a laser to trap the bead and to track the restricted diffusion of the trapped bead. Except to trap the bead using a laser, no other forces are applied on the bead in optical tweezer technique, so that these measurements are representative of passive microrheology, provided the effect of the optical trap is corrected for while estimating the rheological parameters.[16] The motion of the beads is then interpreted in terms of the viscoelastic properties of the surrounding medium. One can also monitor the cross correlated fluctuations of a pair of beads in a dual optical tweezer, whose relative positions varies with time.[15–17]

Rheological characterization of soft materials in bulk yields the viscoelastic parameters of the sample averaged over the volume of the sample studied. The advantage offered by microrheology is that it enables us to characterize the local structural heterogeneity as may be found, in entangled polymer networks such as actin filaments[10] and in silk fibroin solutions,[11] features that bulk measurements may fail to capture. Such a characterization may be of significance in the design of RSF-based gels for biomedical applications. In a previous study, we have carried out a comparative microrheological analysis of RSF solutions obtained from three non-mulberry silk varieties indigenous to the Indian subcontinent viz., Tasar, Eri, and Muga, at a single concentration, and correlated the viscoelastic parameters with their corresponding single fiber stiffness obtained by wide angle X-ray scattering.[12]

In this work, we investigate the rheological behavior of Tasar RSF as a function of concentration. We do so, to examine the propensity of this variety of RSF for gelation and make a comparison with the extensively studied mulberry RSF. We have chosen Tasar RSF for this study as it shows the largest moisture retention as compared with other silk varieties.[3]

The result section of the article is organized as follows: We present a single and dual optical tweezers based microrheological study of Tasar (Karnataka, India) RSF, at a temperature of 22 ± 0.5°C for different concentrations (w/v) and extend the bandwidth down to lower frequencies by including results from video microscopic analysis. The higher frequency bandwidth results are from the optical tweezer based measurements. This study additionally, enables a comparative assessment of the single and dual optical tweezer based methods in obtaining microrheological parameters with this sample in context. Further, the dual tweezer enables, through the correlated measurements of two trapped beads, obtaining the averaged viscoelastic parameters that are more reflective of bulk sample measurements. The increasing opacity of the RSF at higher concentrations results in low signal to noise ratio in monitoring the fluctuations of the probe bead in the sample through quadrant photo diode detectors of optical tweezers and hence at these concentrations, the measurements are restricted to video microscopy.

Sample Preparation

A 3:1 (weight ratio) mixture of calcium nitrate tetrahydrate [$Ca(NO_3)_2$ $4H_2O$] and absolute methanol (CH_3OH) is prepared and is used as a solvent for both non-mulberry and mulberry silk fibers.[18] Raw silk is first degummed thoroughly, as reported elsewhere.[18,19] The degummed silk is cut into small pieces and then added to the solvent. The mixture is stirred well at a temperature of 63°C, until the silk fiber dissolves completely in the solvent to obtain undialyzed RSF. The solutions of a given concentration are prepared by dissolving a known weight of silk in a definite volume of solvent. The RSF solutions at six different concentrations viz., 0.16% (w/v), 0.25% (w/v), 0.50% (w/v), 1.00% (w/v), 2.50% (w/v), and 5.00% (w/v) for Tasar silk, and two concentrations 2.50% (w/v) and 5.00% (w/v) for mulberry silk are prepared with the above procedure. It is observed that the solubility time for the Tasar silk is around 35 min, whereas that for the mulberry silk is around 10 min with this solvent.

Solid polystyrene beads (Cat. no. 17134, 2.799 μm, Polysciences) are mixed with RSF solution in low concentrations (2 μL in 1 mL of RSF). For a uniform distribution of beads in the sample, this gives, inter-bead distances from the centers to be nearly 18 μm. We have observed inter-bead separations in the range from 8 μm to 30 μm in the field of view of our captured Brownian movies of beads embedded in the samples. In case of such inter-bead distances when compared with their diameters, inter-bead interactions are expected to be insignificant. Furthermore, these beads should remain intact and should not be soluble in the sample. When the beads were dispersed in the RSF, they

were indeed found to be insoluble in the sample, as seen from the images of sample observed for 2 h. Polystyrene beads are used as probes to measure the stress-deformation relation in the material. The sample is taken in a well constructed by a rubber "O" ring (10-mm diameter and 2-mm thickness) on a cover slip and is left for 20 min to stabilize before the measurements. For each trial, around 30 μL of sample is used and the temperature is maintained at $22 \pm 0.5^{\circ}$C.

Analysis of the bead fluctuations in video microscopy images shows unrestricted Brownian motions at low concentrations of RSF. This is evidence for the absence of any chemical bond that may link beads to the polymer chain. The restricted motion of beads at higher RSF concentrations is expected due to the increased degree of entanglement in the sample. When the same sample is diluted with the solvent we have observed an increase in the spread of the bead's movement in the sample. This indicates the absence of chemical bonds between the bead and the sample. The chemicals and reagents used in this work were HPLC grade supplied by Merck Chemicals, India.

MEASUREMENT TECHNIQUES

A detailed description of the optical tweezer with image processing setup used in this work can be found elsewhere.[20] We present here the method used in obtaining microrheological parameters.

Optical Tweezer Based Technique

In the optical tweezer technique, for 1-point microrheology, a bead of radius "a" embedded in a given sample is trapped with a laser and the bead's position is tracked either by the same laser or with a different laser back scattered from the trapped bead. A high speed quadrant photo detector (EOS) interfaced with a high speed data acquisition (DAQ) card (PCI 6143, NI), is used to acquire the bead's position with a scan rate of 10^5 samples /sec for 5 s. 20 such data sets are stored on the hard drive of a personal computer, for a given trapped bead, at similar temperatures and surroundings. In 2-point microrheology, two beads, each of radii "a" that are separated by a distance of "r" are trapped by two laser beams (Figure 1) of different planes of polarization. The laser beams backscattered by the two beads, can be separated with the use of a polarizing beam splitter and their positions are recorded simultaneously with two separate detectors as explained in 1-point microrheology. From these data, the auto-correlated power spectral density (PSD) and cross correlated PSD's are calculated using the relations (1 and 2). A detailed procedure for analyzing the data obtained in 2-point microrheology may be found elsewhere.[21] We summarize the salient features of this procedure as below.

The one sided PSD $S_{\alpha}^{(j)}(\omega)$ in 1-point microrheology is defined as,

$$S_{\alpha}^{(j)}(\omega) = \int \langle u_{\alpha}^{(j)}(t) u_{\alpha}^{(j)}(0) \rangle e^{i\omega t} dt \tag{1}$$

and in 2-point microrheology, cross correlated PSDs are given by

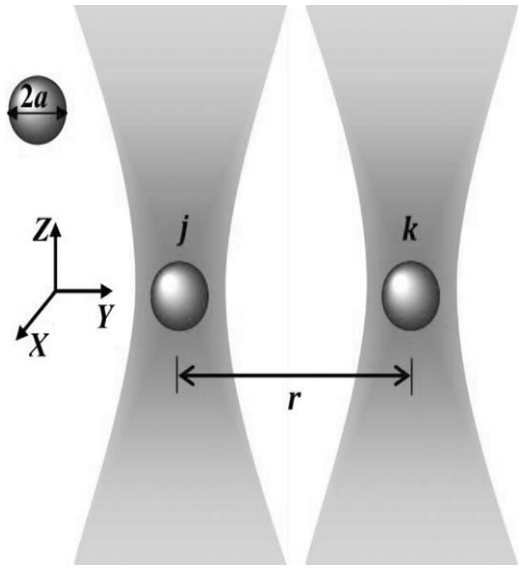

Figure 1. In 2-point microrheology, two beads j and k, each of radii "a" and separated by a distance of "r" are trapped by two laser beams propagating along the "z" direction. Beads' movement in the "xy" plane are tracked by the laser beams backscattered by the two beads, using two independent quadrant detectors.

$$\begin{aligned} S_{||}(\omega) &= \int \langle u_x^{(1)}(t) u_x^{(2)}(0) \rangle e^{i\omega t} dt \\ S_{\perp}(\omega) &= \int \langle u_y^{(1)}(t) u_y^{(2)}(0) \rangle e^{i\omega t} dt \end{aligned} \tag{2}$$

where $u_{\alpha}^{(j)}$ are position fluctuations of a trapped particle in the α directions for the jth particle (1 or 2) α represents the x or y directions of the trapped bead. In 2-point microrheology, cross correlated PSD has two components, one along x direction $S_{||}(\omega)$ and other along y direction $S_{\perp}(\omega)$.

Since the PSD obtained from 1-point as well as 2-point techniques contains the effect of the inherent trap stiffness, the data needs to be corrected for this trap stiffness. The data are corrected for this effect using the standard procedures.[21,22] The microrheological parameters of the medium of interest are calculated using the corrected imaginary response functions "$\chi(\omega)$" with the following relations (3 and 4):

$$\chi_{\text{auto}}(\omega) = \frac{1}{6\pi a G(\omega)} \tag{3}$$

$$\chi_{||}(\omega) = \frac{1}{4\pi r G(\omega)} \;\&\; \chi_{\perp}(\omega) = \frac{1}{8\pi r G(\omega)} \tag{4}$$

where a is the radius of the trapped bead and r is the separation distance between the two trapped particles.

Video Microscopy

Movies containing nearly 1000 images of the freely diffusing, and thermally driven beads in a given medium are stored on to a PC, after focusing the microscope well above (about 20 μm) the cover slip wall to avoid boundary effects.[23] Through multi particle tracking 2–5 beads, embedded in a medium, are tracked simultaneously for each field of view using image analysis algorithms (IDLVM, RSI Systems) to obtain their time-sequenced

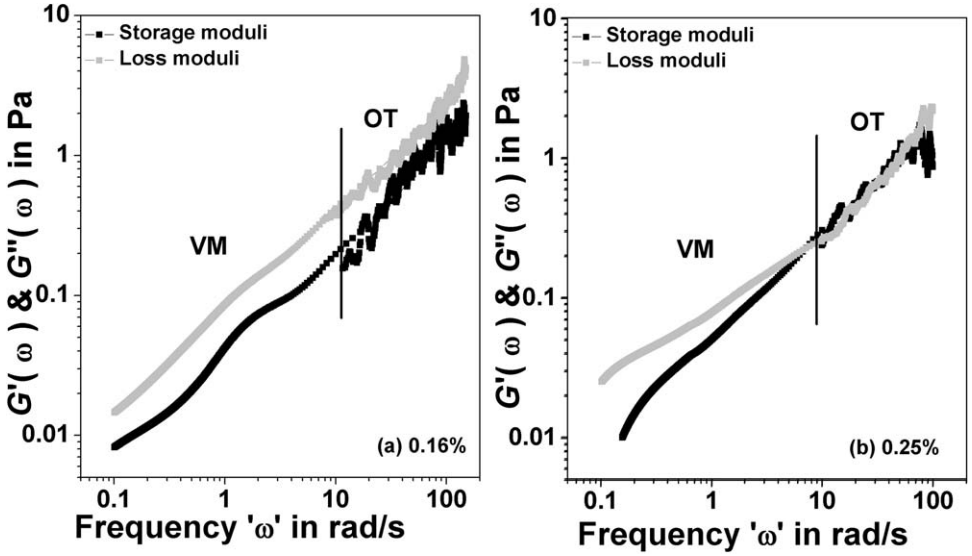

Figure 2. Frequency-dependent loss and storage moduli of Tasar RSF at (a) 0.16 and (b) 0.25 weight percents from video microscopy and optical tweezer techniques. A vertical line drawn in the plot separates the data obtained from the two techniques.

positions.[24,25] The spatial resolution of our imaging system, determined by camera pixel density and optical magnification of the imaging system is 75 nm/pixel at 100 fps.[20]

The position information $r(t)$ of beads embedded in a medium is used to calculate the mean squared displacement (MSD = $\langle \Delta r^2(\tau) \rangle$) of beads in that medium at a temperature T, defined as

$$\langle \Delta r^2(\tau) \rangle = \langle |r(t+\tau) - r(t)|^2 \rangle \tag{5}$$

Here, τ is the lag time, $\langle\rangle$ represents both the average being calculated for all starting times t for a single bead, and the ensemble average of MSD being calculated for a group of beads.[26,27] In each case sample, an ensemble averaged MSD of 25–30 beads is calculated.

For a viscoelastic medium, MSD can be related to the complex shear modulus $G^*(\omega)$ through the generalized Stokes-Einstein relation (GSER) given by[26,27]:

$$G^*(\omega) = \frac{k_B T}{\pi a \langle \Delta r^2(1/\omega) \rangle \Gamma[1+\alpha(\omega)](1+\beta(\omega)/2)} \tag{6}$$

where "$k_B T$" is the thermal energy and $\alpha(\omega)$ and $\beta(\omega)$ are the first and second-order logarithmic time derivatives of the MSD. From the complex shear modulus $G^*(\omega)$ the storage modulus $G'(\omega)$ and loss modulus $G''(\omega)$ of the material are found, by the analytical continuation method[26,27]

$$G'(\omega) = G^*(\omega)\{1/[1+\beta'(\omega)]\}\cos\left[\frac{\pi\alpha'(\omega)}{2} - \beta'(\omega)\alpha'(\omega)\left(\frac{\pi}{2}-1\right)\right]$$
$$G''(\omega) = G^*(\omega)\{1/[1+\beta'(\omega)]\}\sin\left[\frac{\pi\alpha'(\omega)}{2} - \beta'(\omega)[1-\alpha'(\omega)]\left(\frac{\pi}{2}-1\right)\right] \tag{7}$$

where $\alpha'(\omega)$ and $\beta'(\omega)$ are the first and second order logarithmic frequency derivatives of $G^*(\omega)$ and are obtained by fitting the data locally to a second order polynomial. All the microrheological parameters were obtained by the above relations using custom programs, written in LabVIEW.

RESULTS

The rheological properties of Tasar RSF at two weight percents (w/v) 0.16 and 0.25 are measured by both video microscopy and optical tweezer based techniques. In Figure 2, the moduli obtained from both the techniques are superimposed on the same plot for each concentration of Tasar RSF. The video microscopy based data ranges from 0.1 Hz to 10 Hz, while optical tweezer based data ranges from 10 Hz to 100Hz. At a concentration of 0.16% the loss moduli is greater compared with storage moduli at all measured frequencies, a signature of liquid like behavior of the sample. At 0.25 weight percent one can see the slight increase of the storage moduli compared with the loss moduli with the frequency and become nearly the same as that of loss moduli of the sample above 8 rad/sec.

The loss moduli and the storage moduli of Tasar RSF are also determined from the 2-point microrheological technique for the same concentrations and are shown in Figure 3. The values obtained from 2-point microrheological technique are comparable with that of 1-point microrheological technique at all frequencies. These comparable values from the two measurement techniques suggest that at these lower concentrations structural heterogeneities are absent at least up to the measured length scale (4 μm) that is significant in the 2-point technique.[14]

A curve obtained by joining the bead centroids gathered from sequential video images of the fluctuating bead embedded in a RSF sample represents two-dimensional Brownian motion of the embedded bead. To illustrate the types of the bead motions which are embedded in three representative concentrations of the Tasar RSF viz., 0.25 % RSF, 1.0 % RSF and 5.0% RSF are shown in Figure 4 on the same length scale. Figure 4 shows that the embedded bead diffuses relatively to a greater extent in RSF

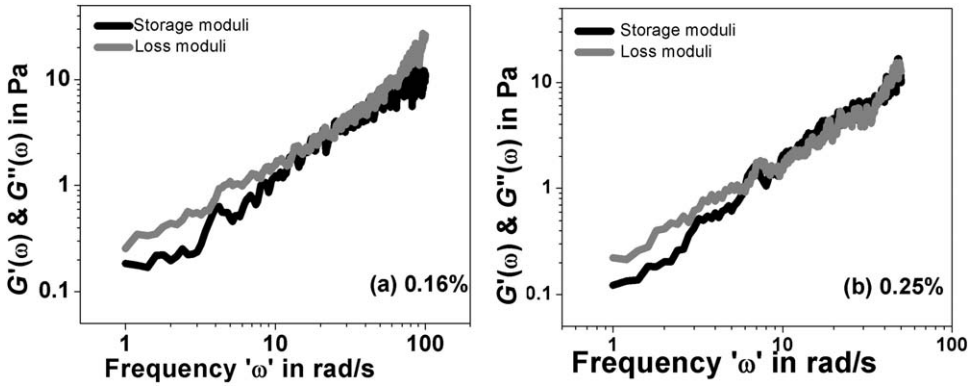

Figure 3. Frequency-dependent loss and storage moduli of Tasar RSF at (a) 0.16 and (b) 0.25 weight percent from optical tweezer based 2-point microrheology technique.

of lower concentrations than in higher concentrations. Fibroin gelation in general, yields a heterogeneous microstructure. In an earlier study it was observed that mulberry RSF exhibit structural heterogeneity at higher concentrations.[11] This behavior is expected to be exhibited even by Tasar RSF at higher concentrations. Therefore a high standard deviation from the ensemble averaged MSD of 25 beads is expected for higher concentrations of RSF.

Figure 5 shows the frequency-dependent loss and storage moduli for five different concentrations namely 0.25%, 0.50%, 1.00%, 2.50%, and 5.00% (w/v) of Tasar RSF solution measured using video microscopy. It is clear that both the storage and loss moduli increase with increase in concentration of the RSF solution, while the cross over frequency decreases with increase in concentration. The loss moduli with increase in concentration shows a relaxation regime that is shifted to lower frequencies, with an intermediate plateau like regime developing, indicative of increasing entanglement in the sample. Similar features have been observed in filamentous bacteriophage fd (fd virus) semi flexible polymers with increase in concentration.[28] A non-chemically crosslinked silk hydrogel sample shows a greater dependency on frequency whereas a crosslinked sample demonstrates nearly constant elastic behavior at all measured frequencies.[9] This indicates that the RSF samples in our study are non-chemically crosslinked samples, and instead, their behavior resembles that of an entangled network structure.[9]

Analysis of Errors

The parameters reported finally, measured using the video microscopy technique include three types of errors. Errors in locating the bead positions in sequenced images are identified as static errors. The static error "$\bar{\varepsilon}$" involved in the measurement is determined by analyzing the ensemble averaged MSD of 30 stuck beads in water, which is nearly 60 nm[29] (see the Supporting Information). The inherent static error of the system seems to be significant at the lower lag times, till about 0.2 s. Beyond that, it has an insignificant effect on the measured MSD. Static error free MSD is obtained by removing the static error present in the measured MSD of free beads, as explained elsewhere.[12,29] In all the samples studied static error corrected MSD is used for further analysis. By properly adjusting the exposure time of the camera magnitude of the dynamic errors in the time lag of sequenced images are minimized.[29]

A second type of error results from the spread of MSDs from individual tracers in the given sample. Ensemble averaging of the MSDs of 25–30 beads reduces the spread in the MSDs of individual tracers in a given sample. This helps to obtain an MSD value of beads embedded in the sample that is used for

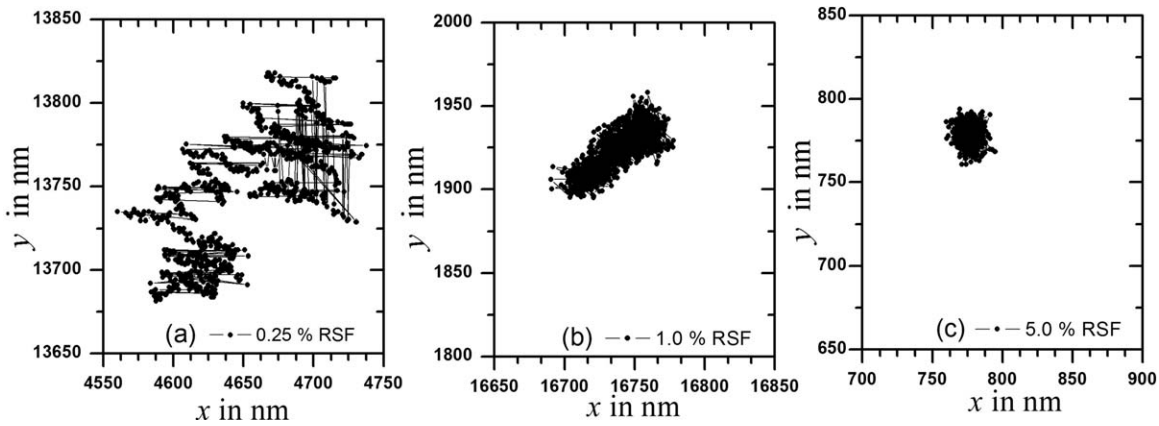

Figure 4. The two-dimensional Brownian motion of beads embedded in (a) 0.25% RSF, (b) 1.0% RSF, and in (c) 5.00% RSF samples shown on the same length scale.

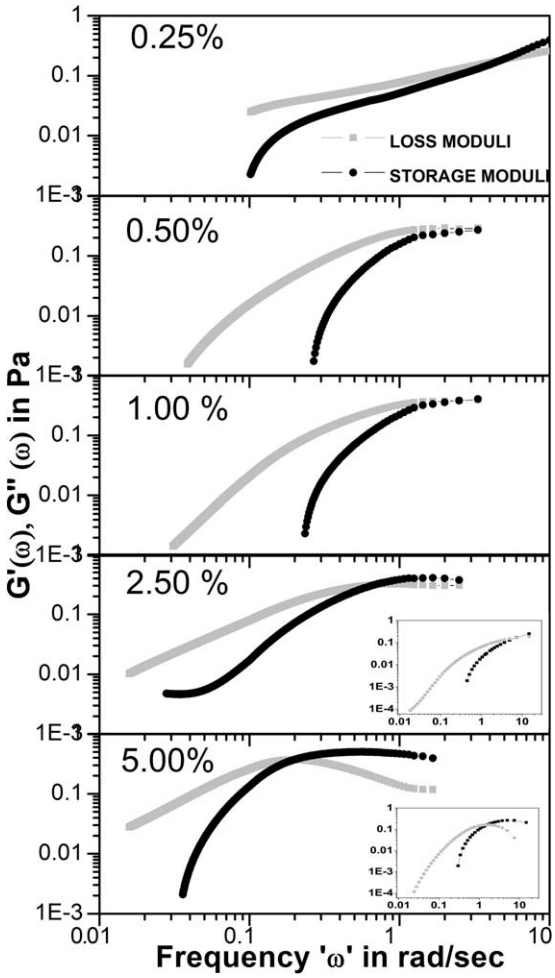

Figure 5. Frequency-dependent loss and storage moduli of Tasar RSF at five different concentrations namely 0.25%, 0.50%, 1.00%, 2.50%, and 5.00% (w/v) obtained from video microscopy. Insets show corresponding values measured in mulberry RSF at these concentrations indicating higher (lower) crossover frequencies (relaxation times).

deriving the rheological parameters of the sample. The viscosity values measured from this method agree well with those from the bulk measurements. In complex fluids, such as Tasar RSF, the standard deviation of MSDs at lower concentrations will be smaller, whereas that at higher concentrations will be larger due to the structural heterogeneity of the sample. The standard deviations of data from the ensemble averaged MSD in water, in 0.50% (w/v) Tasar RSF and in 5.00% (w/v) Tasar RSF are found to be 14%, 24%, and 48% respectively.

Propagation of errors in the individual quantities of relations (7) to (9) gives a measure of the third type of error present in the data. Considering the uncertainties in the bead diameter "a" and in the temperature "T" during our measurements, the errors in the computation of loss and storage moduli can be estimated. The estimated errors in the loss and storage moduli for the two representative concentrations [0.5% and 5.0% (w/v)] are shown in the Figure 6. The magnitude of errors is less than 0.8% in 0.5% RSF and less than 2% in 5.0% RSF. Therefore, these errors are insignificant in our results.

DISCUSSION

The characteristic relaxation time "τ_r" of RSF samples, associated with the large scale motion of the polymer contours is determined using the relation.[30,31]

$$\tau_r = \left(\frac{G'(\omega)}{G''(\omega)}\right)\frac{1}{\omega} \tag{8}$$

Since at cross over frequency $G'(\omega) \approx G''(\omega) \Rightarrow \tau_r = 1/\omega$.

We have also extended measurements on mulberry RSF to examine the trend shown in the relaxation time at higher concentrations. The results from measurements at the higher concentrations are in the insets of Figure 5. The crossover frequency is shifted to lower frequencies for the higher concentrations. Correspondingly, the relaxation time shift to higher values with increase in Tasar RSF concentration as shown in Figure 7. Relaxation time and the values of storage modulus $G'(\omega)$ or loss modulus $G''(\omega)$ at the corresponding crossover frequency for Tasar and mulberry silk fibers are listed in Table II. The characteristic relaxation times for Tasar RSF at higher concentrations namely 2.5% and 5.0% are found to be one order more than that for mulberry RSF at these concentrations. This suggests increased physical cross linking in Tasar RSF as compared with mulberry RSF indicating the initiation of gelation at these concentrations, than that for mulberry RSF.

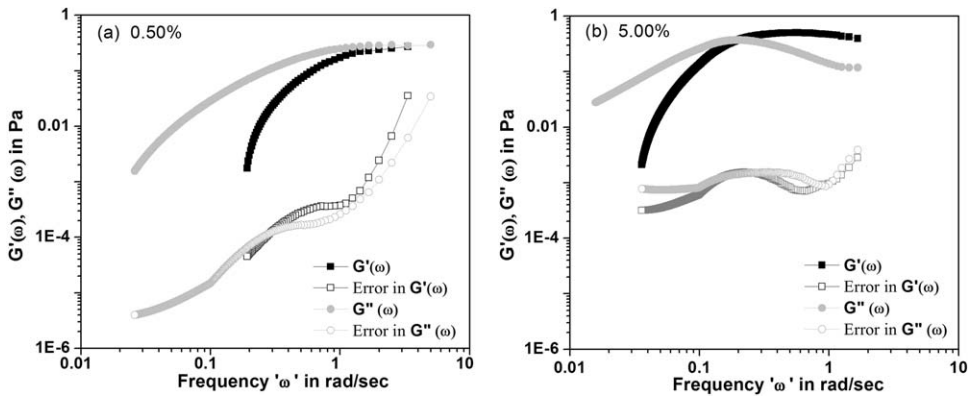

Figure 6. The storage moduli and loss moduli at all measured frequencies along with the magnitude of errors in their estimation in (a) 0.50% RSF and (b) 5.00% RSF.

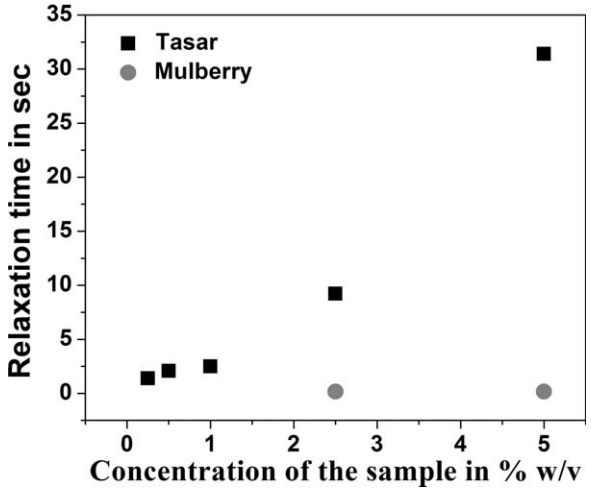

Figure 7. Plot of relaxation time as a function of concentration for two RSF solutions.

We speculate that the relaxation time in Tasar RSF being greater than that of mulberry RSF may be because of the greater stiffness of mulberry silk[2] when compared with the non-mulberry varieties (see Table I). Further, it has been established[2,4] that mulberry silk fibers show higher stress recovery than non-mulberry silk fibers. The fiber that shows greater stiffness is also likely to restore to its initial configuration when the stress is removed, faster than a less stiff fiber. Thus, fibers with lower stiffness can entangle and remain in this configuration longer than their counterparts with greater stiffness. Although the measurement of stiffness has been carried out for macroscopic silk fibers, we expect this relation to hold in the microscopic regime also.[12] Thus, entangled polymer networks of polymer chains with lower stiffness are more likely to show greater relaxation time. In terms of the amino acid content of the fibroins in both varieties, the crystalline regions of the fibroin samples that contain the fully extended chains have smaller peptide units with side groups —H and —CH_2 and preclude the larger amino acid residues with bulkier and polar side groups, which are found in the amorphous regions. The crystalline density is also found to be lower in the non-mulberry varieties as compared with the mulberry silk fibers consequently making the amorphous regions more abundant in the former.[2] Thus, the presence of the larger side groups makes them also more flexible.

Table II. Relaxation Time and the Values of Storage Modulus $G'(\omega)$ or Loss Modulus $G''(\omega)$ at the Corresponding Crossover Frequency for Tasar and Mulberry Silk Fibers

Concentration (w/v)	Relaxation time in seconds		$G'(\omega) = G''(\omega)$ at cross over in Pa	
	Tasar	Mulberry	Tasar	Mulberry
0.25%	1.39		0.175	
0.50%	2.08		0.26	
1.00%	2.50		0.34	
2.50%	9.23	0.9	0.35	0.16
5.00%	31.41	3.9	0.37	0.175

Networks of the semiflexible biopolymers demonstrate high elastic moduli at low polymer volume fractions,[9] and this is reflected in our results, qualitatively, that shows that a smaller volume fraction of Tasar RSF is required to get the required mechanical properties as that compared with mulberry RSF solutions.

A separate plot showing the frequency-dependent storage modulus in Figure 8(a) reveals the plateau region of the curve becoming more prominent with increase in concentration.[32] This feature is also evidence of the increased physical cross linking networks that constrain the motion of the polymer contour. The tendency for gel formation at the same concentrations is thus, greater in Tasar RSF than in mulberry RSF and this may be related to the greater moisture retention as a result of the higher hydrophilic to hydrophobic amino acid content in the former.[3,33]

The damping factor defined as $\tan\delta = [G''(\omega)/G'(\omega)]$ is an indicator of the behavior of Tasar RSF with frequency. A plot of tan δ versus frequency for different RSF concentrations is shown in Figure 8(b). If tan δ is more than 1, then it indicates liquid like behavior. On the other hand if it is less than 1 it indicates solid like behavior.[34] Transition of RSF sample from liquid like

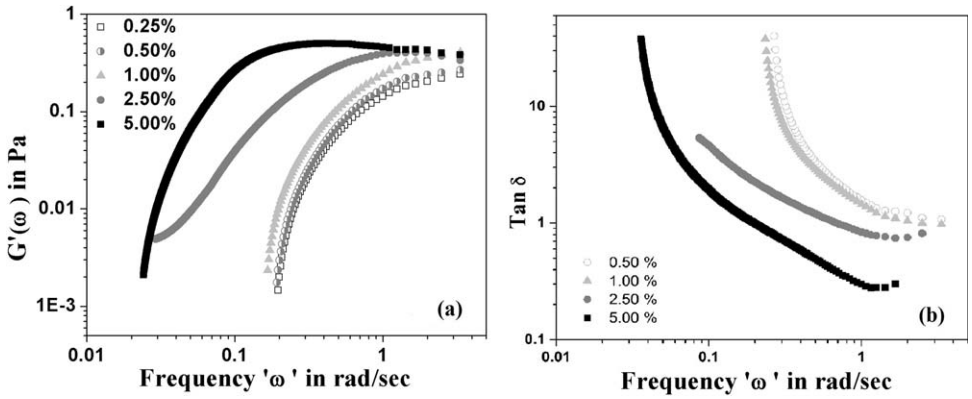

Figure 8. (a) Frequency-dependent storage modulus of Tasar RSF showing increase in plateau region with concentration. (b) A plot of tan $\delta = [G''(\omega)/G'(\omega)]$ as a function of frequency.

behavior to solid like behavior occurs at the crossover frequency, for all RSF concentrations which are determined from Figure 5.

Although silk based gels have the advantage of greater biocompatibility, as when compared with synthetic gels, the rate of silk gelation is slower than the latter.[8] The gelation time depends on many factors and can vary between 4 days to 10 days for different concentrations at room temperature and at pH = 6–8.[8] Tasar RSF samples that we studied were found to form gels around 5–6 days for higher concentrations. This is identified by the increase in the opacity of the sample through the formation of a white opaque compound. This opacity of the sample precluded us from carrying out video microscopic measurements of the Tasar RSF gels. Although, the gelation mechanisms in silk is identified by the increase in the percentage content of β-sheet, even in the fresh silk solutions a combination of non β-sheet forming weak interactions such as hydrogen bonding, hydrophobic and electrostatic interactions do occur.[7,35] These interactions eventually initiate gelation in RSF solutions. These inter and intramolecular interactions lead to physical cross links (entanglement) that subsequently lead to β-sheet conformations in silk solutions.[7] Increased fibroin concentration provides a situation for increased chain interactions and thus accelerates gelation.[9] This explains the increased storage moduli with concentration. To the best of our knowledge such characterization of Tasar has not been carried out so far.

Limited transparency of the RSF at concentrations greater than 5% made it difficult to employ video microscopy to examining this process further. Furthermore, handling low volumes at higher concentrations is an issue, as the beads do not disperse in the medium uniformly.[23] At above 5% RSF concentration, we found that the beads do not uniformly disperse throughout the volume of the sample. This may be because of the increasing viscoelastic nature of the sample at these concentrations rendering it difficult for the probe beads to move to different regions of the sample volume. Nonetheless, the relaxation times that are an order of magnitude greater at the higher measured concentrations for Tasar RSF than for mulberry RSF indicate that Tasar RSF is a better gel former than mulberry RSF.

CONCLUSIONS

We have measured the viscoelasticity of RSF solution of Tasar silk for six concentrations. It is observed that both frequency-dependent loss and storage moduli increase with increase in concentration. The loss moduli are more than the storage moduli till the crossover frequency after which the storage moduli becomes dominant over loss moduli at all frequencies. The dependency of storage and loss moduli on frequencies displays the behavior that exhibited by entangled networks. The relaxation time is found to be greater in Tasar RSF than that in mulberry RSF. The onset of gelation in Tasar RSF at a concentration of 5.0%, indicates the potential of Tasar RSF as a gel for future biomedical applications. These results are examined in relation to the viscoelastic parameters of mulberry silk, wherein the larger crossover frequencies at the same higher concentrations indicate relaxation times that are smaller than those measured for Tasar RSF.

ACKNOWLEDGMENTS

The authors acknowledge a project grant from the Department of Science and Technology, Government of India (Nano mission programme) that enabled this work. We thank Professor G. Subramanya, University of Mysore, for donating the silk fibers used in this work.

REFERENCES

1. Xu, Y.; Zhang, Y.; Huilishao Hu, X.C. *Int. J. Biol. Macromolecules* **2005**, *35*, 155.
2. Rajkhowa, R.; Gupta, V. B.; Kothari, V. K. *J. Appl. Polym. Sci.* **2000**, *77*, 2418.
3. Sen, K.; Murugesh, Babu, K. *J. Appl. Polym. Sci.* **2004**, *92*, 1080.
4. Kothari, V. K.; Rajkhowa, R.; Gupta, V. B. *J. Appl. Polym. Sci.* **2001**, *82*, 1147.
5. Raghu, A.; Ananthamurthy, S. *Bull. Mater. Sci.* **2008**, *31*, 359.
6. Mackintosh, F. C.; Kas, J.; Janmey, P. A. *Phys. Rev. Lett.* **1995**, *75*, 4425.
7. Ayub, Z. H.; Arai, M.; Hirabayashi, K. *Biosci. Biotech. Biochem.* **1993**, *57*, 1910.
8. Matsumoto A.; Chen, J.; Collette, A.; Kim, U-J.; Altman, G. H.; Cebe, P.; Kaplan, D. *J. Phys. Chem. B* **2006**, *110*, 21630.
9. Rammensee, S.; Huemmerich, D; Hermanson, K; Scheibel, T; Bausch, A. R. *Appl Phys. A* **2006**, *82*, 261.
10. Apgar, J.; Tseng, Y.; Federov, E.; Herwig, M. B.; Almo, S. C.; Wirtz, D. *Biophys. J.* **2000**, *79*, 1095.
11. Raghu, A.; Somashekar, R.; Ananthamurthy, S. *J. Polym. Sci. Part B: Polym. Phys.* **2007**, *45*, 2555.
12. Divakara, S.; Raghu, A.; Roy, S.; Yogesh A.; Somashekar, R.; Ananthamurthy, S. *Indian J. Fiber Text. Res.* **2008**, *34*, 168.
13. Waigh, T. A. *Rep. Prog. Phys.* **2005**, *68*, 685.
14. Mason, T. G.; Weitz, D. A. *Phys. Rev. Lett.* **1995**, *74*, 1250.
15. Crocker, J. C.; Valentine, M. T.; Weeks, E. R.; Gisler. T.; Kaplan, P. D.; Yodh, A. G.; Weitz, D. A. *Phys. Rev. Lett.* **2008**, *85*, 888.
16. Atakhorami, M.; Schmidt, C. F. *Rheol. Acta.* **2006**, *45*, 449.
17. Starrs, L.; Bartlett, P. *Faraday Discuss.* **2003**, *123*, 323.
18. Xin, C.; Knight, D. P.; Shao, Z.; Vollrath, F. *Polymer.* **2001**, *42*, 9969.
19. Sohn, S.; Strey, H. H.; Gido, S. P. *Biomacromolecules.* **2004**, *5*, 751.
20. Yogesh, A.; Raghu, A.; Nagesh, B. V.; Bhattacharya, S.; Mohana, D. C.; Sharath, A. *Int. J. Nanosci.* **2011**, *10*, 181.
21. Atakhorrami, M.; Sulkowska, J. I.; Addas, K. M.; Koenderink, G. H.; Tang, J. X.; Levine, A. J.; MacKintosh, C.; Schmidt, C. F. *Phys. Rev. E.* **2006**, *73*, 061501.
22. Gittes, F.; Schnurr, B.; Olmsted, F.; MacKintosh, C.; Schimdt, C. F. *Phys. Rev. Lett.* **1997**, *79*, 3286.
23. Breedveld, V.; Pine, D. J. *J. Mater. Sci.* **2003**, *38*, 4461–4470.
24. Crocker, J. C.; Grier, D. G. *J. Colloid Interface Sci.* **1996**, *179*, 298.

25. IDLVM Code. Available at: http://titan.iwu.edu/~gspaldin/rytrack.html. Accessed on June 25 2008.
26. Mason, T. G. *Rheol. Acta*. **2000**, *39*, 371.
27. Dasgupta, B. R.; Tee, S. Y.; Crocker, J. C.; Frisken, B. J.; Weitz, D. A. *Phys. Rev. E.* **2002**, *65*, 051505-(1–10).
28. Addas, K. M.; Schmidt, C. F.; Tang, J. X. *Phys. Rev. E*, **2004**, *70*, 021503 (1).
29. Savin, T.; Doyle, P. S. *BioPhys. J.* **2005**, *88*, 623.
30. Dealy, J. M.; Larson, R. G. *Structure and Rheology of Molten Polymers: From Structure to Flow Behaviour and Back Again; Hanser Publishers, Munich*, **2006**.
31. Rubinstein, M.; Colby, R. H.; Polymer Physics; Oxford University Press: Oxford, **2003**.
32. Doi, M.; Edwards, S. F. The Theory of Polymer Dynamics; Oxford University Press: Oxford, **1986**.
33. Andrew, P. N.; Victor, B.; Lisa, P.; Bulent, O.; Pine, D. J.; Darrin, P.; Timothy, J. D. *Nature*, **2002**, *417*, 424.
34. Oppong, F. K.; Rubatat, L.; Frisken, B. J.; Baily, A. E.; de Bruyn, J. R. *Phys. Rev. E*, *73*, 041405.
35. Kim, U. J.; Park, J.; Li, C.; Jin, H. J.; Valluzzi, R.; Kaplan, D. L. *Biomacromolecules*, **2004**, *5*, 786.